AIAA JOURNAL
Vol. 49, No. 3, March 2011

Piezoelectric Transducer Diagnostics via Linear Reciprocity for Guided Wave Structural Health Monitoring

Sang Jun Lee* and Jennifer E. Michaels†
Georgia Institute of Technology, Atlanta, Georgia 30332-0250
Hoon Sohn‡
Korea Advanced Institute of Science and Technology, Daejeon 305-701, Republic of Korea
and
Thomas E. Michaels§
Georgia Institute of Technology, Atlanta, Georgia 30332-0250

DOI: 10.2514/1.J050733

Guided waves using spatially distributed piezoelectric transducers are being applied to many structural health monitoring applications. These surface-mounted transducers, which are typically lead zirconate titanate, are generally assumed to be both undamaged and properly bonded to the host structure during usage. However, this assumption may not be valid, particularly after long-term operation under realistic environmental conditions. The transducer integrity becomes even more critical for aerospace applications because of the inevitably harsh operational conditions. In this study, a methodology for piezoelectric transducer diagnosis is developed to identify both damaged and poorly bonded transducers by quantifying the degree of signal reciprocity for guided waves propagating between pairs of surface-mounted transducers. The proposed method does not require direct comparison of signals to baselines, and it is independent of structural complexities such as geometrical features and boundaries. The method is also insensitive to environmental and operational conditions, such as temperature and applied loads, and is therefore not susceptible to false alarms caused by such variations. The efficacy of the proposed diagnostic technique is evaluated via two-dimensional simulations followed by experiments under varying environmental and operational conditions for piezoelectric transducers mounted on an aluminum plate.

Nomenclature

A	=	antisymmetric Lamb wave modes
a	=	half-length of transducer A
B	=	beta function
b	=	half-length of transducer B
$\bar{b}$	=	half-length of bond of partially debonded transducer B
d	=	half-thickness of specimen
E^{rms}	=	signal change index
F	=	transducer damage index
g_{31}	=	xz-directional piezoelectric constant
h_{A}	=	thickness of transducer A
h_{B}	=	thickness of transducer B
M	=	number of transducer transducers
S	=	symmetric Lamb wave modes
V_{AB}	=	signal from transducer A to transducer B
V_{BA}	=	signal from transducer B to transducer A
x_{AB}	=	distance between transducer A and transducer B
Y_p	=	Young's modulus of lead zirconate titanate
y	=	confidence level of beta distribution
α	=	shape parameter of beta distribution
β	=	shape parameter of beta distribution
κ_{AB}	=	coupling function to the specimen when debonded transducer B is used as a sensor
κ_{BA}	=	coupling function to the specimen when debonded transducer B is used as an actuator
λ	=	Lamé constant
μ	=	Lamé constant
ξ	=	wave number for antisymmetric and symmetric Lamb wave modes
ρ	=	specimen density
χ_F	=	threshold level of transducer damage classifier

Received 12 July 2010; revision received 21 October 2010; accepted for publication 5 November 2010.

*Postdoctoral Fellow, School of Electrical and Computer Engineering. Member AIAA.
†Associate Professor, School of Electrical and Computer Engineering.
‡Associate Professor, Civil and Environmental Engineering Department.
§Professor of the Practice, School of Electrical and Computer Engineering.

I. Introduction

GUIDED waves are being evaluated to detect defects for structural health monitoring (SHM) applications, and piezoelectric materials such as lead zirconate titanate (PZT) are widely applied, as reported in the review article by Raghavan and Cesnik [1]. Kessler and Spearing [2] applied PZT transducers to implement a guided wave-based structural damage detection method for composites, for which the usage in aerospace structures is rapidly increasing. Cuc et al. [3] also proposed several guided wave-based SHM techniques using PZT transducers, which were tested on complex metallic structures similar to aircraft panels. When a PZT transducer is used for SHM, it is generally assumed that it is perfectly bonded to the structure and that its bonding condition does not deteriorate throughout its usage. It is also assumed that the transducer itself does not experience any damage such as partial fractures, cracks, and detachment from the host structure. However, these assumptions may not be valid after the transducer has been in service for many years, especially when PZT-based SHM systems are applied to aerospace applications that normally include harsh external conditions. Anton et al. [4] recently reported a damage detection method using instantaneous baseline measurements. They applied PZT sensor diagnostics after mounting the transducers but not during structural monitoring for damage.

Most existing transducer diagnosis techniques are based upon electromechanical impedance methods, as reported by multiple researchers [4–8], and transducer defects are identified by comparing current data obtained from a potentially damaged transducer with prior baseline data measured when the transducer was in pristine condition. However, direct comparisons between current and

baseline data can result in false alarms because of unavoidable sensitivity of signals to operational, structural, and environmental variations. For example, Park et al. [9] showed that comparison of electromechanical impedance spectra requires application of temperature compensation techniques for reliable performance. A reference-free concept for guided wave-based structural damage detection was first developed by Kim and Sohn [10], and this concept was extended for PZT transducer diagnosis by Lee and Sohn [11]. This guided wave-based technique uses minimal baseline data and does not require any temperature compensation techniques. However, it does rely on edge reflections acquired from each sensor operating in pulse–echo mode (i.e., self-sensing), and thus may not be generally applicable.

In this study, a guided wave-based PZT diagnosis methodology is developed to identify transducer defects without direct use of baseline data. This method can be easily applied to a spatially distributed PZT array, such as reported in [12], without the additional electronics required for impedance measurements or the self-sensing method developed by Lee and Sohn [11]. The advantage of the proposed technique is that abnormal transducers that are operating in conjunction with intact transducers can be detected even when the structure is subjected to varying operational, environmental, and structural conditions, regardless of the structure's geometrical complexity.

To achieve this goal, the proposed diagnosis technique uses linear reciprocity of guided wave propagation between pairs of surface-bonded PZT transducers. If two PZT transducers are said to be identical, it is implied that not only do their PZT elements have the same properties, but their sizes and bonding conditions are also identical. If one PZT transducer is used as an actuator and a second identical transducer is used as a sensor, and vice versa, the two measured time responses between them are reciprocal because of the reciprocity theorem for a linear system [13]. However, if two PZT transducers are not identical because of PZT cracking, one of the PZTs is reduced in area compared with the other, and there is an amplitude difference between the two time responses to conserve the energy transmission ratio. Or, if two PZT transducers are not identical because of PZT debonding, there is a difference between the shape of the two time responses as well as the amplitudes because the vibration of the debonded PZT area and the bad coupling with the structure disturb the actuation and sensing. Consequently, the two signals between them are not reciprocal. The proposed technique, which is an extension of work reported in [14,15], identifies the abnormal PZT transducer pair by a quantitative comparison of the two measured time responses.

This paper first introduces the theoretical development of the reciprocity-based PZT transducer diagnostics and proposes a PZT damage index. Then, two-dimensional (2-D) numerical simulations are presented between two surface-bonded PZT transducers. Experiments are performed with a PZT transducer array bonded to an aluminum plate under varying temperature and structural conditions. Finally, results are reported and concluding remarks are made.

II. Theory

In this section, the theoretical basis for linear reciprocity-based PZT diagnosis is explained. First, the case of signals propagating between two intact and well-bonded PZT transducers is considered. Next, the case of signals propagating between an intact PZT and a cracked PZT is presented, where a cracked PZT is modeled as a well-bonded PZT with a reduced area. Then, the case of signals traveling between an intact PZT and a debonded PZT is considered. Finally, the PZT damage identification method is proposed, which consists of a signal change index, a corresponding PZT damage index, and an outlier analysis to establish the threshold.

A. Two Well-Bonded Transducers

Here, the responses of Lamb waves between two well-bonded PZT transducers are introduced, as shown in [13]. Based on the theory for selective Lamb wave mode excitation [16,17], it is assumed that a 2-D PZT actuator creates surface shear stress $\tau = \tau_0[\delta(x-a) - \delta(x+a)]e^{i\omega t}$ along its edges, where ω is the angular frequency of harmonic excitation. As derived in [17], signals V_{AB} and V_{BA}, obtained between two intact PZT transducers (PZT A and PZT B), are

$$V_{\mathrm{AB}}(t) = \frac{\tau_0 Y_P h_{\mathrm{A}} h_{\mathrm{B}} g_{31}}{\mu}\left[\sum_{\xi^S}\frac{\sin(\xi_S a)}{\xi_S}\frac{\sin(\xi_S b)}{2b}\frac{N_S(\xi_S)}{D'_S(\xi_S)}e^{i(\xi_S x_{\mathrm{AB}}-\omega t)} + \sum_{\xi^A}\frac{\sin(\xi_A a)}{\xi_A}\frac{\sin(\xi_A b)}{2b}\frac{N_A(\xi_A)}{D'_A(\xi_A)}e^{i(\xi_A x_{\mathrm{AB}}-\omega t)}\right] \tag{1}$$

$$V_{\mathrm{BA}}(t) = \frac{\tau_0 Y_P h_{\mathrm{A}} h_{\mathrm{B}} g_{31}}{\mu}\left[\sum_{\xi^S}\frac{\sin(\xi_S b)}{\xi_S}\frac{\sin(\xi_S a)}{2a}\frac{N_S(\xi_S)}{D'_S(\xi_S)}e^{i(\xi_S x_{\mathrm{AB}}-\omega t)} + \sum_{\xi^A}\frac{\sin(\xi_A b)}{\xi_A}\frac{\sin(\xi_A a)}{2a}\frac{N_A(\xi_A)}{D'_A(\xi_A)}e^{i(\xi_A x_{\mathrm{AB}}-\omega t)}\right] \tag{2}$$

where

$$\alpha^2 = \frac{\omega^2}{c_L^2} - \xi^2, \qquad \beta^2 = \frac{\omega^2}{c_T^2} - \xi^2$$
$$c_L = \sqrt{\frac{\lambda+2\mu}{\rho}}, \qquad c_T = \sqrt{\frac{\mu}{\rho}} \tag{3}$$

$$N_S = \xi^S\beta(\xi_S^2+\beta^2)\cos\alpha d\cos\beta d$$
$$D_S = (\xi_S^2-\beta^2)^2\cos\alpha d\sin\beta d + 4\xi_S^2\alpha\beta\sin\alpha d\cos\beta d \tag{4}$$

and

$$N_A = \xi^A\beta(\xi_A^2+\beta^2)\sin\alpha d\sin\beta d$$
$$D_A = (\xi_A^2-\beta^2)^2\sin\alpha d\cos\beta d + 4\xi_A^2\alpha\beta\cos\alpha d\sin\beta d \tag{5}$$

Note that D'_S and D'_A represent the derivatives of D_S and D_A with respect to the wave number. Here, signal V_{AB} denotes the response signal measured at PZT B when the input signal is applied to PZT A, and signal V_{BA} is defined in a similar manner. If PZT A and PZT B are the same size ($a = b$) and have the same bonding condition, the output responses, V_{AB} and V_{BA}, are also identical, as can be seen by comparing Eqs. (1) and (2). On the other hand, if one of the PZT transducers has a crack, then $a \neq b$, and the output responses V_{AB} and V_{BA} show only an amplitude difference.

B. One Well-Bonded and One Debonded Transducer

The debonded PZT transducer has a different bonded area compared with that of the intact PZT transducer, which affects the output responses. In the case of the intact PZT actuator and the debonded PZT sensor, the input energy transmitted into the host structure is identical to the case of the intact PZT actuator and sensor. However, in the case of the debonded PZT actuator and the intact PZT sensor, the input energy is smaller than that of the former case because of the bad coupling of the debonded PZT actuator with the structure. The corresponding signals V_{AB} and V_{BA} can be expressed as

$$V_{\mathrm{AB}}(t) = \kappa_{\mathrm{AB}}(\bar{b}, b, \omega, t)\frac{\tau_0 Y_P h_{\mathrm{A}} h_{\mathrm{B}} g_{31}}{\mu} \times \left[\sum_{\xi^S}\frac{\sin(\xi_S a)}{\xi_S}\frac{\sin(\xi_S \bar{b})}{2\bar{b}}\frac{N_S(\xi_S)}{D'_S(\xi_S)}e^{i(\xi_S x_{\mathrm{AB}}-\omega t)} + \sum_{\xi^A}\frac{\sin(\xi_A a)}{\xi_A}\frac{\sin(\xi_A \bar{b})}{2\bar{b}}\frac{N_A(\xi_A)}{D'_A(\xi_A)}e^{i(\xi_A x_{\mathrm{AB}}-\omega t)}\right] \tag{6}$$

$$V_{\mathrm{BA}}(t) = \kappa_{\mathrm{BA}}(\bar{b}, b, \omega, t)\frac{\tau_0 Y_{\mathrm{P}} h_{\mathrm{A}} h_{\mathrm{B}} g_{31}}{\mu} \times \left[\sum_{\xi^S}\frac{\sin(\xi_S \bar{b})}{\xi_S}\frac{\sin(\xi_S a)}{2a}\frac{N_S(\xi_S)}{D'_S(\xi_S)}e^{i(\xi_S x_{\mathrm{AB}}-\omega t)} + \sum_{\xi^A}\frac{\sin(\xi_A \bar{b})}{\xi_A}\frac{\sin(\xi_A a)}{2a}\frac{N_A(\xi_A)}{D'_A(\xi_A)}e^{i(\xi_A x_{\mathrm{AB}}-\omega t)}\right] \quad (7)$$

The functions κ_{AB} and κ_{BA} capture the effect of poor coupling on signals V_{AB} and V_{BA}, respectively, because of the partial debond of PZT B. Since $a \neq \bar{b}$ and the coupling coefficients are frequency dependent, the output responses V_{AB} and V_{BA} are different in both shape and amplitude.

C. Transducer Damage Identification

First, to quantitatively compare the signals between the two PZTs, a signal change index E^{rms} is calculated:

$$E^{\mathrm{rms}}_{\mathrm{AB}} = \sqrt{\frac{\sum_t [V_{\mathrm{AB}}(t) - V_{\mathrm{BA}}(t)]^2}{\sqrt{\sum_t [V_{\mathrm{AB}}(t)]^2}\sqrt{\sum_t [V_{\mathrm{BA}}(t)]^2}}} \quad (8)$$

If normal variations of E^{rms} for an intact PZT pair are known, E^{rms} can be readily examined to determine whether the two PZTs have the same condition or if one of them is damaged. Note that it cannot be determined which one of the pair is damaged from only the signal change index.

Next, to automatically identify abnormal PZT(s) among an array of spatially distributed PZTs, a damage index F is defined for each PZT from the error indices between all possible pairs in the array:

$$F_i = \min_{j, j\neq i}[E^{\mathrm{rms}}_{ij}] \quad (9)$$

where i and j indicate the ith and jth PZTs. It is expected that all of the E^{rms} values of the pairs containing the damaged PZT will be relatively large, resulting in a large F value for the abnormal PZT that can be clearly identified.

For practical purposes, the E^{rms} values between intact PZTs fall between zero and one, because the signals being compared are generally in phase and are of similar amplitude. Values can exceed one when a transducer is completely disconnected, one signal is smaller than half of the other signal, or the shapes are very different, all of which would indicate a problem that is not expected for intact PZTs. Thus, a beta distribution [18] is used to model the statistical distribution of F values for initially intact PZT transducers. The procedure is to fit the beta distribution to the F values obtained from the intact PZT transducers and then set a threshold level χ_F that corresponds to a specific confidence level y:

$$\chi_F = \frac{1}{\mathrm{B}(\alpha, \beta)} y^{\alpha-1}(1-y)^{\beta-1} \quad (10)$$

Here, α and β are estimated from the F index values obtained from the baseline data at 21°C, and a threshold value (χ_F) corresponding to a one-sided 99.9% confidence interval is computed at the upper tail of the distribution. When an F value exceeds this threshold level, it is considered as an outlier, and the associated PZT transducer is classified as damaged.

To summarize, once the threshold level has been determined, the proposed PZT damage identification process consists of the following four steps:

1) Measure all possible time signals between PZT pairs (a total of $M(M-1)$ signals for M PZTs).

2) Calculate the E^{rms} value for each pair (a total of $M(M-1)/2$ values).

3) Find the minimum E^{rms} value (F) among the computed E^{rms} values that are associated with a specific PZT. Repeat this calculation for each PZT (M F_i values, one for each of the M PZTs).

4) Detect outliers among the F values using the predetermined threshold level to identify any abnormal PZTs.

III. Simulations

For the numerical simulations, a 2-D aluminum plate of 305 × 6.35 mm was considered, as shown in Fig. 1. The COMSOL 3.5a Multiphysics software[¶] was used to simulate Lamb wave propagation in a 2-D aluminum plate using the plain strain, piezoplain strain, and electrostatics modules of the software. Two PZT transducers were attached on the top surface of the plate, and the thickness of the adhesive layer was 0.1 mm. The nominal material properties were used for the aluminum, adhesive, and PZT layers [19]. A 250 kHz five-cycle tone-burst signal with an amplitude of ±10 V was applied to the top electrode of one of the PZT transducers, and the corresponding output signal was measured with the other PZT transducer. In the simulation, the 250 kHz driving frequency was selected so that only S_0 and A_0 modes were generated. The simulation results were obtained using a time-dependent solver with the time step set to 0.1 μs, which is equivalent to 10 MHz. To control the error in each integration step, relative and absolute tolerances for the solution were chosen to be 10^{-4} and 10^{-10}, respectively. To simulate PZT debonding, the bonding layer of PZT B was shortened to 50% of the PZT length. Similarly, to simulate PZT cracking, the lengths of both the bonding layer and the PZT were shortened to 50% of their initial lengths.

Figure 2 shows 2-D numerical results for the signals recorded between the two PZT transducers. As expected for two identical PZTs, signals AB and BA are identical in Fig. 2a. The corresponding E^{rms} value is 0.0297, which is close to zero. Note that the model discretization error produced a relatively small residual signal. In contrast, Figs. 2b and 2c show significant residual signals for which the amplitudes and shapes depend on the size of the cracked and debonded PZTs, which produce E^{rms} values of 1.2706 and 1.6529, respectively. These results show potential that the proposed technique can identify when two PZTs have different conditions.

IV. Experiments

In this section, various experiments are performed to evaluate the proposed PZT diagnostic procedure. First, the time responses between two PZTs are shown for different PZT conditions. Then, a spatially distributed PZT array is tested under both varying temperature and applied loads.

A. Experimental Setup

Circular PZTs of 7 mm diameter and 0.5 mm thickness were used to validate the efficacy of the proposed technique. Three different PZT transducer conditions were prepared, as previously described in [11]. To summarize, a piece of commercial Teflon tape was partially inserted between the PZT transducer and the plate to simulate PZT debonding. After the bonding layer was cured, the tape was removed. The PZT transducer was subsequently cracked using a razor blade.

The data acquisition system, which consisted of a controller, an arbitrary waveform generator, a multiplexer, an amplifier, and a digitizer, was controlled by a custom LabVIEW® program. A 250 kHz tone-burst signal with an amplitude of ±10 V was generated with a resolution of 16 bits and a sampling rate of 20 MHz. This signal was applied to either PZT A or PZT B via the multiplexer. The output signal was filtered and amplified by 32 dB and then digitized with a resolution of 14 bits at 20 MHz. Fifty signals were averaged to improve the signal-to-noise ratio, and the repetition rate was limited to 20 Hz to avoid signal wraparound.

B. Time Responses Between Two Transducers

Measured signals are shown in Fig. 3, corresponding to intact transducers and two cases of transducer damage. Details of the simulated and experimental signals differ because the simulated

[¶]Data available at http://www.comsol.com [retrieved 24 June 2010].

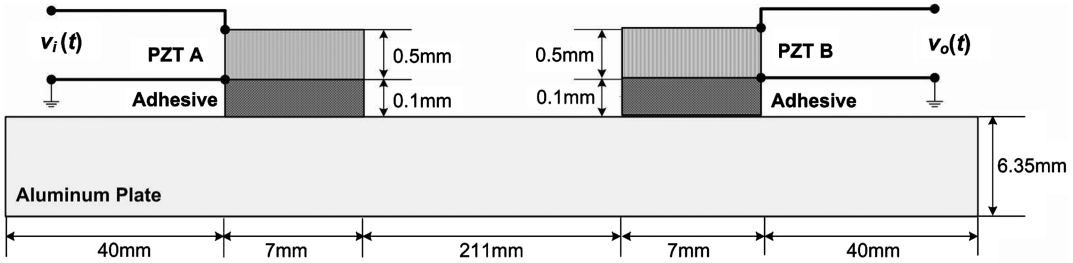

Fig. 1 Dimensions and configuration of the 2-D structure, adhesive, and PZT transducers used for the numerical simulations (not to scale).

signals were based upon a 2-D model, whereas the experimental signals were recorded from a finite three-dimensional (3-D) plate. As expected, the two time response signals measured between two identical PZT transducers (PZT A and PZT B) are reciprocal, as shown in Fig. 3a. The corresponding E^{rms} value is 0.013, which is close to zero. In contrast, if two PZT transducers have different sizes caused by cracking or debonding defects, the two time response signals are significantly different from each other, as shown in Figs. 3b and 3c, with E^{rms} values of 0.166 and 0.201, respectively. A likely explanation for the smaller E^{rms} values for the experiments, as compared with the simulations, is the difference between the 2-D PZT model and the 3-D nature of the actual circular PZT transducers. In addition, even though 50% cracking or debonding was intended during sensor preparation, the severity of actual PZT damage could be less.

C. Varying Temperature

As the temperature is increased or decreased, individual echoes shift in time because of a combination of specimen volume change and change in wave speed. Also, temperature affects the PZT capacitance values and results in an amplitude change of the time response, as reported in [11]. These temperature-induced shape and amplitude variations make a direct comparison to a baseline impractical, because such comparisons can require both additional baselines and nontrivial postprocessing via temperature compensation techniques, as shown in [20–22]. However, the proposed diagnostic technique is expected to be insensitive to temperature variations, because it uses only the currently measured time responses to calculate the signal change index and the corresponding PZT damage index.

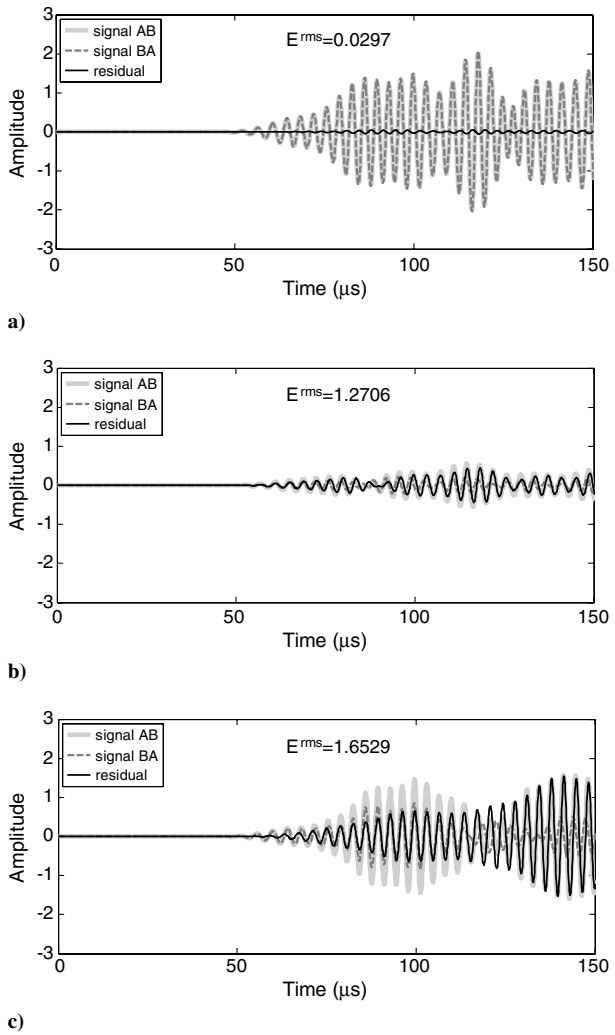

Fig. 2 Signals between two PZTs from 2-D numerical simulations: a) two intact PZTs, b) intact PZT and 50% cracked PZT, and c) intact PZT and 50% debonded PZT.

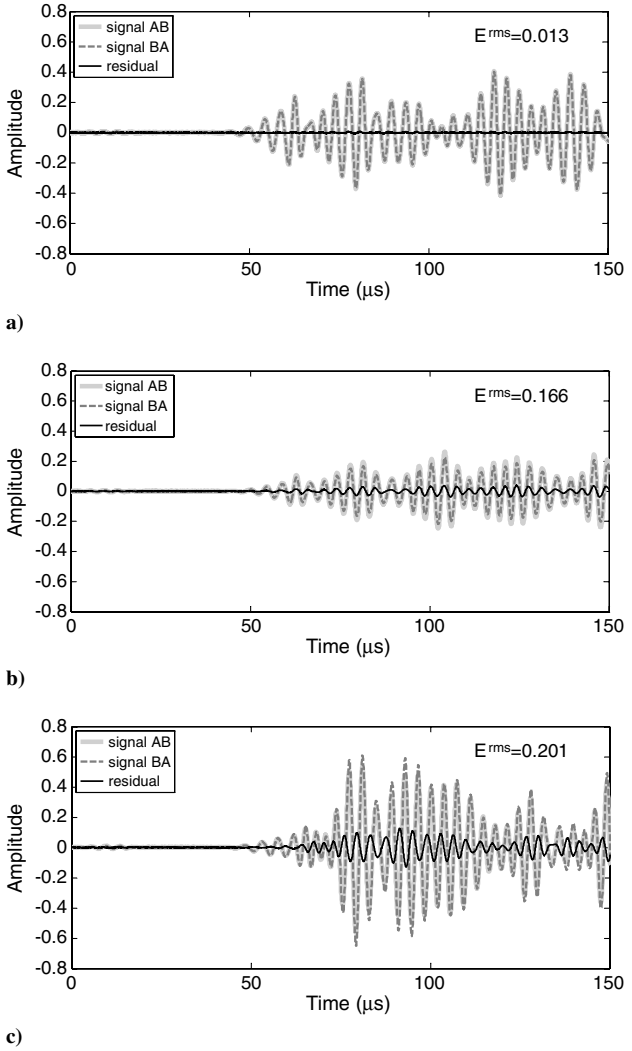

Fig. 3 Signals from experiments between two PZTs for a 250 kHz tone-burst excitation: a) two intact PZTs, b) one intact and one cracked PZT, and c) one intact and one debonded PZT.

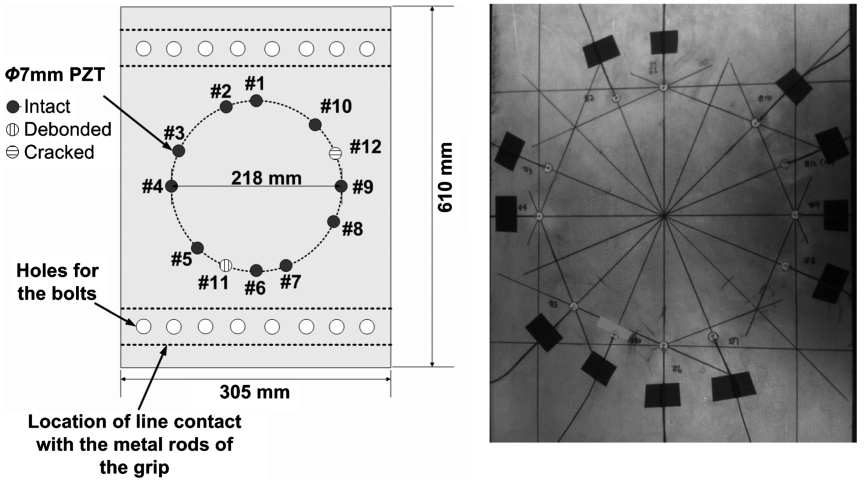

Fig. 4 Aluminum plate of dimensions 305 × 610 × 6.35 mm with 12 surface-bonded PZT transducers. The sketch on the left is not to scale, and the photograph is of the sensor area only.

Figure 4 shows a sketch and photograph of the 12 PZT transducers that were bonded with epoxy to an aluminum plate of dimensions 305 × 610 × 6.35 mm. PZT 11 was debonded by about 50% of its area, and PZT 12 was cracked, also by about 50% of its area; all other PZTs were intact. The effect of temperature changes on the measured signals from one transducer pair (PZTs 1 and 6) is shown in Fig. 5 for three different temperatures (16, 21, and 31°C) and, as expected, it can be seen that the primary effect is to stretch the signal with little distortion. However, these small amplitude and phase changes could result in false alarms of the current PZT state if an approach based on a direct comparison to baseline signals is used for PZT diagnostics.

Next, the feasibility of the proposed PZT diagnosis method is demonstrated for the three different temperature conditions. Figure 6a shows calculated E^{rms} values for the three temperatures. Note that 36 pairs (72 time signals) were measured instead of all 66 possible pairs to reduce the total time for data acquisition. The pairs were randomly chosen with the constraint that each PZT be included in six pairs, and Table 1 relates pair numbers to the individual PZTs. The E^{rms} values for sensor pair 1 (PZTs 1 and 6) for 16, 21, and 31°C are 0.021, 0.017 and 0.018, respectively. These small values demonstrate that the proposed E^{rms} index is insensitive to temperature. Figure 6b shows the corresponding F values. The beta distribution parameters were determined from the 10 F values corresponding to the 10 undamaged PZTs (1–10) at 21°C, and the threshold level was calculated from Eq. (10) with $y = 99.9\%$. The F values from the 10 intact PZT transducers are below the threshold, and those from the two damaged PZTs are well above the threshold for all three temperatures.

Finally, the effect of the length of the time window was considered for all 12 PZTs, with results shown in Fig. 7. As expected, the time window does not affect performance of the proposed technique, which is advantageous in practice because the user does not need to adjust or tune this parameter. Note that each time window has its own threshold level; they are almost identical and are not shown in Fig. 7.

D. Varying Loads

Stresses arising from normal operational conditions of a structure, such as during takeoffs, landings, and in-flight maneuvering of an aircraft, are expected to significantly change guided wave signals. As

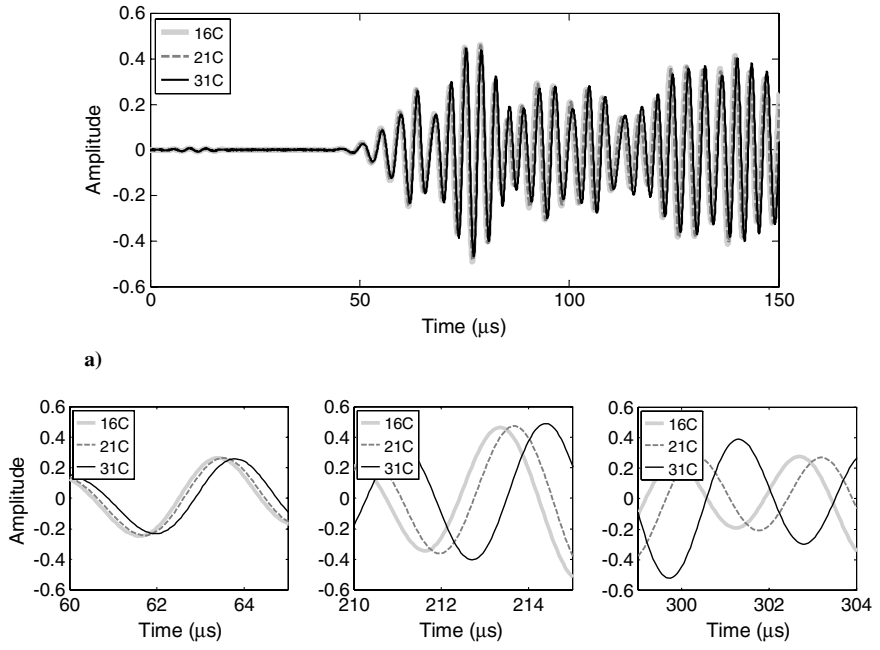

Fig. 5 The effect of temperature changes on the measured signals from one transducer pair: a) signals obtained between PZTs 1 and 6 under varying temperatures, and b) zoomed views of the signals illustrating the stretching effect caused by a homogeneous temperature increase.

Table 1 Relationship between pair numbers and PZT numbers

Pair Number	PZT Numbers	Pair Number	PZT Numbers	Pair Number	PZT Numbers
1	1–6	13	2–5	25	5–8
2	1–7	14	2–6	26	5–9
3	2–7	15	2–8	27	5–12
4	1–8	16	2–11	28	6–10
5	5–10	17	3–6	29	6–12
6	2–9	18	3–7	30	7–9
7	3–8	19	3–11	31	7–10
8	3–9	20	3–12	32	7–12
9	4–9	21	4–6	33	8–11
10	1–4	22	4–8	34	9–11
11	1–5	23	4–10	35	10–11
12	1–10	24	4–12	36	11–12

the stress is increased or decreased, each echo shifts in time due to both dimensional variations and changes of wave speeds with stress (the acoustoelastic effect). These effects are shown in [23] for bulk waves and [24] for guided waves. Since the time shifts depend upon the direction of propagation, direct comparisons to baselines can be even more problematic than for temperature changes.

To investigate the sensitivity of the proposed PZT diagnosis method to changing stresses, measurement were made with a spatially distributed PZT array under varying uniaxial loads. Here, the same specimen as shown in Fig. 4 with 12 bonded PZTs was used, and six different static tensile stresses from 0 to 57.5 MPa were applied with the setup shown in Fig. 8. Note that, in addition to the load-induced dimension and wave speed changes, there may also be significant boundary condition changes at the grips that affect reflections of the Lamb waves. Also, the stress level of a PZT transducer may alter its piezoelectricity and consequently affect the response signal.

The effect of loading on the measured signals was first considered for three different static loading conditions. As shown in Fig. 9, the initial arrival behaves the same as for a temperature change, which is a simple time shift as the load changes. However, because of the anisotropy of the applied load, later arrivals are no longer simply shifted or stretched by an amount proportional to the arrival time. Consequently, the amount of the shift is generally unpredictable, and some parts of the signal may show significant shape changes so that it is not possible to identify a simple time shift. Grip variations may also cause unpredictable signal changes. As is the case for temperature variations, both amplitude and phase changes induced by applied loads could also cause false alarms of the current PZT state if an approach based on a direct comparison to baseline signals is used for PZT diagnostics. Although all values are not shown, the E^{rms} values for the sensor pair 1 (PZTs 1 and 6) for loads of 0, 23, and 46 MPa are 0.022, 0.020 and 0.021, respectively. These small values confirm that the proposed E^{rms} index is insensitive to varying loading conditions.

Variations of the F values under different loading conditions are compared to examine the effect of loading on the proposed PZT diagnosis technique. As shown in Fig. 10, the proposed PZT damage index performs properly under different stresses. Also, the F values are not sensitive to the PZT locations and angles with respect to the loading direction. Note that the F values for PZTs 8, 9, and 10 are close to the threshold level. It is speculated that their bonding conditions may have degraded somewhat during the loading tests because; as can be seen by their F values in Fig. 6b, their initial bonding conditions were worse than the other PZTs.

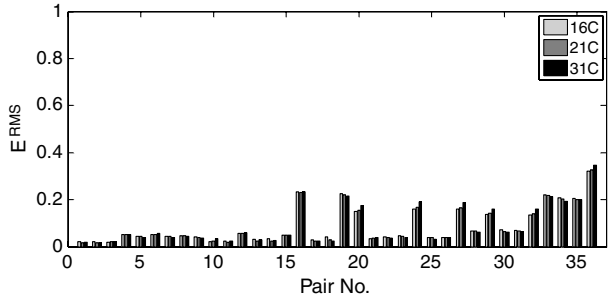

a)

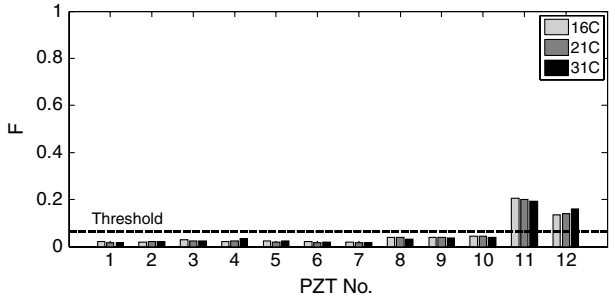

b)

Fig. 6 PZT damage identification with a 500 μs time window and a 250 kHz tone-burst excitation: a) signal change index (E^{rms}) values, and b) corresponding PZT damage index (F) values.

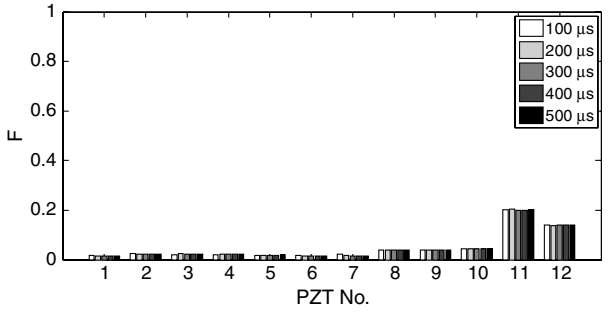

Fig. 7 PZT damage identification using five different time windows. Note that there are five corresponding threshold levels that are intentionally not shown.

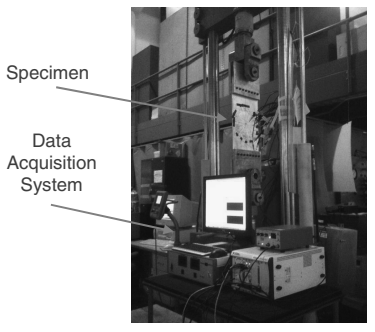

Fig. 8 Test setup for variable loading experiments.

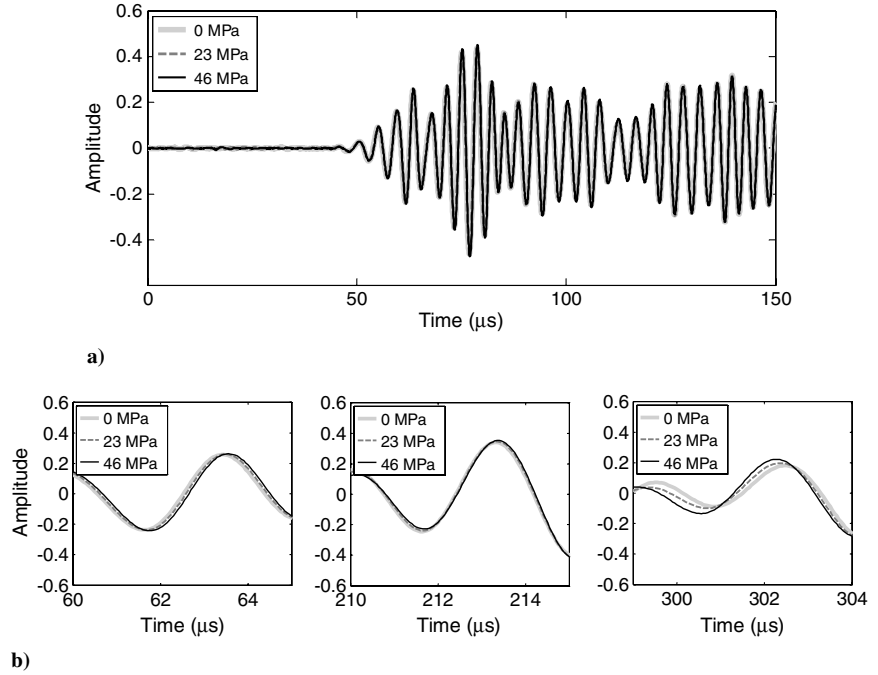

Fig. 9 The effect of loading on the measured signals from one transducer pair: a) signals between PZTs 1 and 6 for a 250 kHz tone-burst excitation under static loading conditions, and b) zoomed views of the signals at different time windows illustrating the complicated effects of an applied uniaxial load.

Multiple loading experiments were performed to investigate the reliability of the proposed technique. After the second loading test, the F value for PZT 4 exceeded the threshold, as shown in Fig. 11. It was found that the wire connected to the bottom (ground) electrode of PZT 4 was disconnected, which resulted in significant noise in the measured signal, especially when PZT 4 was used as a sensor (receiver). This result indicates that the proposed technique may also be used to detect electrical connection problems, although these are not specifically considered here. After the wire was reattached, repeatability was excellent.

E. Effect of Excitation Frequency

In the previous subsection, the driving frequency was 250 kHz, which generates only the fundamental Lamb wave modes (A_0 and S_0). Prior results reported in [13,14], obtained at 150 kHz (which also includes just the fundamental Lamb wave modes), show comparable performance to the 250 kHz results reported here. Two additional driving frequencies are considered that include higher order modes, both under varying temperatures. Based on theoretical dispersion curves for the tested aluminum plate, a driving frequency of 400 kHz can generate A_0, S_0, and A_1 Lamb wave modes, and 600 kHz can

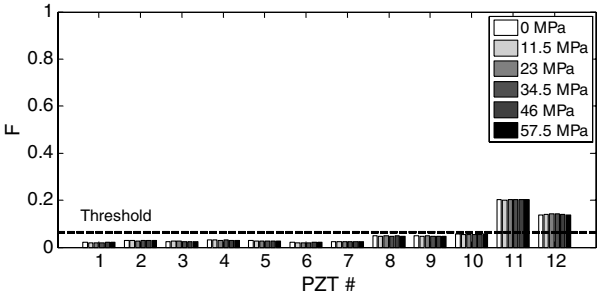

Fig. 10 PZT damage identification for different tensile stresses at 250 kHz. The threshold level was determined from PZTs 1–10 at 21°C and 0 MPa. Note that PZTs 11 and 12 are damaged.

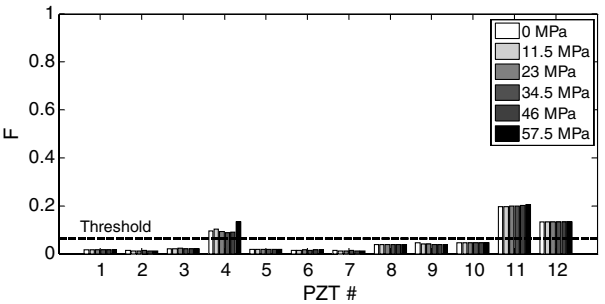

Fig. 11 PZT damage identification with additionally damaged PZT 4 for different tensile stresses at 250 kHz. The threshold level is the same as for Fig. 10, and PZTs 11 and 12 are damaged.

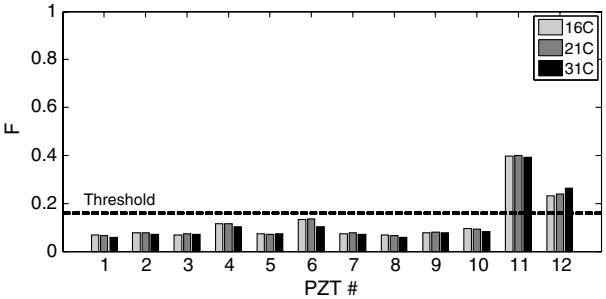

Fig. 12 PZT damage identification for three different temperature conditions at 400 kHz. The threshold level was determined from PZT 1–10 at 21°C and 0 MPa. Note that PZTs 11 and 12 are damaged.

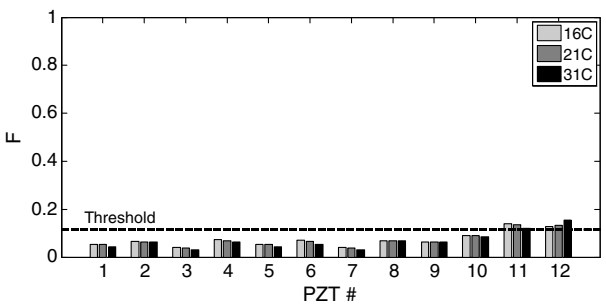

Fig. 13 PZT damage identification for three different temperature conditions at 600 kHz. The threshold level was determined from PZT 1–10 at 21°C and 0 MPa. Note that PZTs 11 and 12 are damaged.

generate A_0, S_0, A_1, and S_1 modes. Figures 12 and 13 show the results for these two cases. Note that the threshold levels for both 400 and 600 kHz are markedly higher than for the 250 kHz experiments, which could indicate a combination of increased nonlinearities and lower signal-to-noise ratios at higher frequencies. For the 400 kHz results of Fig. 12, the damaged PZTs are still readily detected because their F values when damaged are also higher than those from the 250 kHz experiments. For the 600 kHz results of Fig. 13, the damaged PZTs are also detected, but their F values barely exceed the threshold, indicating that this frequency choice will most likely be unduly sensitive to noise and unlikely to reliably detect small transducer defects.

V. Conclusions

In this study, a guided wave-based method to detect PZT transducer defects without any direct comparison with baseline signals is proposed and implemented. This diagnosis technique is based upon linear reciprocity of guided wave propagation between pairs of identical surface-mounted PZT transducers, and it is particularly suitable for a spatially distributed PZT array where all possible reciprocity pair combinations are considered. The main advantages of the proposed technique are its effectiveness under varying operational, environmental, and structural conditions, and its insensitivity to geometrical complexity and edge reflections. Furthermore, it can be easily applied to an existing PZT-based SHM system without additional equipment, such as an electronic circuit or an impedance analyzer. The feasibility of the proposed technique was successfully verified through both numerical simulations and experiments using circular PZT transducers bonded to an aluminum plate under varying temperatures and loading conditions.

One parameter that should be carefully considered is the frequency of excitation. Preliminary experimental results indicate that sensitivity to PZT damage may be compromised at higher frequencies, which may not be a problem when using the fundamental Lamb wave modes. Another issue that should be investigated in future research is quantifying the level of PZT damage that can be both detected and tolerated. Here, the damage was rather large (i.e., 50% of the transducer area for both debonded and cracked PZTs), and it was not considered if smaller levels of PZT damage could be detected before such damage impacts the performance of the SHM system.

There are several limitations to the proposed method. First, two transducers that have exactly the same type and severity of damage cannot be detected, because there will still be signal reciprocity between them. Second, there must be at least two undamaged transducers in the network. For example, if there are a total of three transducers, with one undamaged and two damaged, the proposed method will produce erroneous results, either reporting only the undamaged transducer as damaged or no damaged transducers at all. The likelihood of these situations is expected to be relatively low for many practical implementations, and they could, furthermore, be effectively addressed by complementary methods, such as those described in [11,19].

Acknowledgments

This work was partially sponsored by the U.S. Air Force Office of Scientific Research, Structural Mechanics Division, grant number FA9550-08-1-0241, and the U.S. Air Force Research Laboratory under contract number FA8650-09-C-5206. This work was also partially supported by the Radiation Technology Program (M20703000015-07N0300-01510) and the Nuclear Research and Development Program (2009-0083489) of the National Research Foundation of Korea under the Ministry of Education, Science, and Technology.

References

[1] Raghavan, A., and Cesnik, C. E. S., "A Review of Guided-Wave Structural Health Monitoring," *Shock and Vibration Digest*, Vol. 39, No. 2, 2007, pp. 91–114. doi:10.1177/0583102406075428

[2] Kessler, S., and Spearing, M. S., "In-Situ Sensor-Based Damage Detection of Composite Materials for Structural Health Monitoring," 43rd AIAA/ASME/ASCE/AHS/ASC Structures, Structural Dynamics, and Materials Conference, Denver, CO, AIAA Paper 2002-1545, 2002.

[3] Cuc, A., Giurgiutiu, V., Joshi, S., and Tidwell, Z., "Structural Health Monitoring with Piezoelectric Wafer Active Sensors for Space Applications," *AIAA Journal*, Vol. 45, No. 12, 2007, pp. 2838–2850. doi:10.2514/1.26141

[4] Anton, S., Inman, D., and Park, G., "Reference-Free Damage Detection Using Instantaneous Baseline Measurements," *AIAA Journal*, Vol. 47, No. 8, 2009, pp. 1952–1964. doi:10.2514/1.43252

[5] Park, G., Farrar, C. R., Rutherford, A. C., and Robertson, A. N., "Piezoelectric Active Sensor Self-Diagnostics Using Electrical Admittance Measurements," *Journal of Vibration and Acoustics*, Vol. 128, No. 4, 2006, pp. 469–476. doi:10.1115/1.2202157

[6] Giurgiutiu, V., Zagrai, A., and Bao, J. J., "Piezoelectric Wafer Embedded Active Sensors for Aging Aircraft Structural Health Monitoring," *Structural Health Monitoring*, Vol. 1, No. 1, 2002, pp. 41–61. doi:10.1177/147592170200100104

[7] Saint-Pierre, N., Jayet, Y., Perrissin-Fabert, I., and Baboux, J. C., "The Influence of Bonding Defects on the Electric Impedance of Piezoelectric Embedded Element," *Journal of Physics D: Applied Physics*, Vol. 29, No. 12, 1996, pp. 2976–2982. doi:10.1088/0022-3727/29/12/006

[8] Eckstein, B., Fritzen, C. P., and Bach, M., "Advancements in Self-Diagnosis of Bonded Piezoelectric Transducers," *Proceedings of the 4th European Workshop on Structural Health Monitoring*, edited by T. Uhl, DEStech Publ., Lancaster, PA, 2008.

[9] Park, G., Kabeya, K., Cudney, H. H., and Inman, D. J., "Impedance-Based Structural Health Monitoring for Temperature Varying Applications," *JSME International Journal, Series A: Mechanics and Material Engineering*, Vol. 42, No. 2, 1999, pp. 249–258.

[10] Kim, S. B., and Sohn, H., "Instantaneous Reference-Free Crack Detection Based on Polarization Characteristics of Piezoelectric Materials," *Smart Materials and Structures*, Vol. 16, No. 6, 2007, pp. 2375–2387. doi:10.1088/0964-1726/16/6/042

[11] Lee, S. J., and Sohn, H., "Piezoelectric Transducer Self-Diagnosis Under Changing Environmental and Structural Conditions," *IEEE Transactions on Ultrasonics, Ferroelectrics, and Frequency Control*, Vol. 57, No. 9, 2010, pp. 2017–2027. doi:10.1109/TUFFC.2010.1649

[12] Michaels, J. E., "Detection, Localization and Characterization of Damage in Plates With an In Situ Array Of Spatially Distributed Ultrasonic Sensors," *Smart Materials and Structures*, Vol. 17, No. 3, 2008, Paper 035035. doi:10.1088/0964-1726/17/3/035035

[13] Achenbach, J. D., *Reciprocity in Elastodynamics*, Cambridge Univ. Press, Cambridge, England, U.K., 2004.

[14] Lee, S. J., Sohn, H., Michaels, J. E., and Michaels, T. E., "In Situ Detection of Surface-Mounted PZT Transducer Defects Using Linear Reciprocity," *Review of Progress in Quantitative Nondestructive Evaluation*, edited by D. O. Thompson and D. E. Chimenti, Vol. 29, American Inst. of Physics, College Park, MD, 2010, pp. 1844–1851. doi:10.1063/1.3362311

[15] Lee, S. J., Michaels, J. E., Michaels, T. E., and Sohn, H., "In Situ PZT Diagnostics Using Linear Reciprocity Under Environmental and Structural Variations," *Proceedings of the SPIE: Health Monitoring of Structural and Biological Systems*, Vol. 7650, SPIE, 2010, Paper 76500N. doi:10.1117/12.847326

[16] Giurgiutiu, V., and Lyshevski, S. E., *Micromechatronics: Modeling, Analysis, and Design with MATLAB*, 1st ed., CRC Press, Boca Raton, FL, 2003, Chap. 11.

[17] Raghavan, A., and Cesnik, C. E. S., "Modeling of Piezoelectric-Based Lamb-Wave Generation and Sensing for Structural Health Monitoring," *Proceedings of the SPIE*, Vol. 5391, SPIE, 2004, pp. 419–430. doi:10.1117/12.540269

[18] Park, W. J., and Kil, R. M., "Pattern Classification with Class Probability Output Network," *IEEE Transactions on Neural Networks*, Vol. 20, No. 10, 2009, pp. 1659–1673. doi:10.1109/TNN.2009.2029103

[19] Lee, S. J., Sohn, H., and Hong, J.-W., "Time Reversal Based Piezoelectric Transducer Self-Diagnosis Under Varying Temperature," *Journal of Nondestructive Evaluation*, Vol. 29, No. 2, 2010, pp. 75–91. doi:10.1007/s10921-010-0067-3

[20] Lu, Y., and Michaels, J. E., "A Methodology for Structural Health Monitoring with Diffuse Ultrasonic Waves in the Presence of Temperature Variations," *Ultrasonics*, Vol. 43, No. 9, 2005, pp. 717–731.
doi:10.1016/j.ultras.2005.05.001

[21] Konstantinidis, G., Drinkwater, B. W., and Wilcox, P. D., "The Temperature Stability of Guided Wave Structural Health Monitoring Systems," *Smart Materials and Structures*, Vol. 15, No. 4, 2006, pp. 967–976.
doi:10.1088/0964-1726/15/4/010

[22] Clarke, T., Cawley, P., Wilcox, P. D., and Croxford, A. J., "Evaluation of the Damage Detection Capability of a Sparse-Array Guided Wave SHM System Applied to a Complex Structure Under Varying Thermal Conditions," *IEEE Transactions on Ultrasonics, Ferroelectrics, and Frequency Control*, Vol. 56, No. 12, 2009, pp. 2666–2678.
doi:10.1109/TUFFC.2009.1357

[23] Mi, B., Michaels, J. E., and Michaels, T. E., "An Ultrasonic Method for Dynamic Monitoring of Fatigue Crack Initiation and Growth," *Journal of the Acoustical Society of America*, Vol. 119, No. 1, 2006, pp. 74–85.
doi:10.1121/1.2139647

[24] Michaels, J. E., Lee, S. J., and Michaels, T. E., "Effects of Applied Loads and Temperature Variations on Ultrasonic Guided Waves," *Proceedings of the 5th European Workshop on Structural Health Monitoring*, Sorrento, Italy, DEStech Publ., Lancaster, PA, 2010, pp. 1267–1272.

A. Palazotto
Associate Editor